Effects of Molecular Structure and Interfacial Ligation on the Precision of Cu-Bound α,ω-Mercaptoalkanoic Acid "Molecular Ruler" Stacks

ARTICLE *in* LANGMUIR · FEBRUARY 2007

Impact Factor: 4.46 · DOI: 10.1021/la0621719 · Source: PubMed

4 AUTHORS, INCLUDING:

Gregory S Mccarty
North Carolina State University
32 PUBLICATIONS **927** CITATIONS
SEE PROFILE

David L Allara
Pennsylvania State University
261 PUBLICATIONS **23,213** CITATIONS
SEE PROFILE

Effects of Molecular Structure and Interfacial Ligation on the Precision of Cu-Bound α,ω-Mercaptoalkanoic Acid "Molecular Ruler" Stacks

Thomas A. Daniel, Sundarajan Uppili, Gregory McCarty,† and David L. Allara*

Department of Chemistry and The Materials Research Institute, The Pennsylvania State University, University Park, Pennsylvania 1680

Received July 24, 2006. In Final Form: September 25, 2006

Nanolithography processes based on designed, precision thickness multilayer thin films (molecular rulers) have been reported that enable patterning of features on surfaces from a few to the hundred nanometer range. These strategies are unique in their potential ability to enable wafer scale patterning of features of just a few nanometers. If these techniques could be developed to be sufficiently precise and generally applicable, they would fill a long-standing need in nanoscience. In this study a systematic and detailed analysis of the growth mechanisms and molecular layer structures has been carried out for the mercaptoalkanoic acid−copper ion multilayer thin film system currently used as the standard nanolithography resist. Our results show these films form via a redox reaction of thiol groups with surface-ligated Cu(II) ions to form adlayers at only ∼50% coverage with islanding of the alkyl chains, thereby leading to rough topographies and less than theoretical thicknesses based on a 1:1 ideal adlayer. Strategies are suggested to help overcome these issues for molecular resist applications in nanolithographic processing.

1. Introduction

The use of self-assembled, multilayer molecular films as precision spacers ("molecular rulers") for lithographic processing has been reported recently.[1−6] These reports indicate that appropriate molecular ruler films (MRFs), in conjunction with lift-off or other standard lithographic techniques, can be used on surfaces with nominal micrometer scale patterns (prepared, e.g., by standard photolithography) to create final topographical features in the 1−100 nm width range. Such a capability, if sufficiently precise and generally applicable, would fill a long-standing gap in patterning by providing designed, precision dimensions down to the molecular scale.

The present state-of-the-art is based on alkanethiol−gold chemistry and thus presently is limited to patterning gold features,[1−6] though suitable chemistries should allow extensions to other materials. In detail, multilayer stacks of self-assembled monolayers (SAMs), each with a predesigned thickness, are formed layer by layer on a foundation SAM of an ω-carboxy-alkanethiolate SAM on Au{111} [$HO_2C(CH_2)_nS-$/Au].[7] The foundation SAM is prepared on a surface with gold features, e.g., micrometer-width gold posts or lines on a silicon oxide substrate, with the SAM forming selectively on and conformal to the gold features. While a number of methods are available for forming conformal multilayers,[8−17] the current work is based on the method developed by Ulman and co-workers[8] which uses stacks of α,ω-mercaptoalkanoic acid layers ligated at their interfaces by copper ions. The self-assembly was proposed[8] to follow steps represented schematically in Figure 1. Once the foundation SAM is formed, by iterations of the subsequent steps with selected constituent molecules of specific molecular lengths the thickness of the final stack, in principle, can be precisely controlled. Following the current reports,[1−6] a typical patterning process would involve (1) fabrication of gold features on the oxide layer of a silicon substrate, (2) selective formation of a conformal MRF stack, terminated by a simple alkanethiol SAM, on the gold features, (3) vapor deposition of gold over the entire surface, and (4) removal of the gold (lift-off) selectively from the low-energy MRF surface. In this mode the MRF acts as a release agent. This process results in formation of a new gold feature formed between the original ones with original−new feature separation gaps determined by the selected thickness of the MRF stack. As a final step the feature edges can be cleaned by oxidative or other methods. Variations of the process steps can be designed to give different types of new features and gaps.

The success of MRFs in forming precision nanometer scale features with sharp, highly replicating feature edges and gap widths will depend critically on the ability to control the precision

* To whom correspondence should be addressed. E-mail: dla3@psu.edu.

† Present address: North Carolina State University and University of North Carolina, Chapel Hill, 2140 Burlington Laboratories, North Carolina State University, Raleigh, NC 27695.

(1) Hatzor, A.; Weiss, P. S. *Science* **2001**, *291* (5506), 1019−1020.

(2) Anderson, M. E.; Tan, L. P.; Tanaka, H.; Mihok, M.; Lee, H.; Horn, M. W.; Weiss, P. S. *J. Vac. Sci. Technol., B* **2003**, *21* (6), 3116−3119.

(3) Anderson, M. E.; Smith, R. K.; Donhauser, Z. J.; Hatzor, A.; Lewis, P. A.; Tan, L. P.; Tanaka, H.; Horn, M. W.; Weiss, P. S. *J. Vac. Sci. Technol., B* **2002**, *20* (6), 2739−2744.

(4) Anderson, M. E.; Srinivasan, C.; Jayaraman, R.; Weiss, P. S.; Horn, M. W. *Microelectron. Eng.* **2005**, *78*−*79* 248−252.

(5) McCarty, G. S. *Nano Lett.* **2004**, *4*, 1391−1394.

(6) Anderson, M. E.; Mihok, M.; Tanaka, H.; Tan, L.-P.; Horn, M. W.; McCarty, G. S.; Weiss, P. S. *Adv. Mater.* **200**6, *18*, 1020−1022.

(7) Nuzzo, R. G.; Dubois, L. H.; Allara, D. L. *J. Am. Chem. Soc.* **1990**, *112*, 558−569.

(8) Evans, S. D.; Ulman, A.; Goppertberarducci, K. E.; Gerenser, L. J. *J. Am. Chem. Soc.* **1991**, *113* (15), 5866−5868.

(9) Freeman, T. L.; Evans, S. D.; Ulman, A. *Langmuir* **1995**, *11* (11), 4411−4417.

(10) Brust, M.; Blass, P. M.; Bard, A. J. *Langmuir* **1997**, *13* (21), 5602−5607.

(11) Auer, F.; Nelles, G.; Sellergren, B. *Chem.−Eur. J.* **2004**, *10* (13), 3232−3240.

(12) Cheng, W. L.; Dong, S. J.; Wang, E. K. *Chem. Mater.* **2003**, *15* (13), 2495−2501.

(13) Lee, H.; Kepley, L. J.; Hong, H. G.; Mallouk, T. E. *J. Am. Chem. Soc.* **1988**, *110* (2), 618−620.

(14) Lee, H.; Kepley, L. J.; Hong, H. G.; Akhter, S.; Mallouk, T. E. *J. Phys. Chem.* **1988**, *92* (9), 2597−2601.

(15) Tillman, N.; Ulman, A.; Penner, T. L. *Langmuir* **1989**, *5* (1), 101−111.

(16) Ansell, M. A.; Zeppenfeld, A. C.; Yoshimoto, K.; Cogan, E. B.; Page, C. J. *Chem. Mater.* **1996**, *8* (3), 591−594.

(17) Zhang, W. W.; Lu, C. S.; Zou, Y.; Xie, J. L.; Ren, X. M.; Zhu, H. Z.; Meng, Q. J. *J. Colloid Interface Sci.* **2002**, *249* (2), 301−306.

10.1021/la0621719 CCC: $37.00
Published on Web 11/21/2006

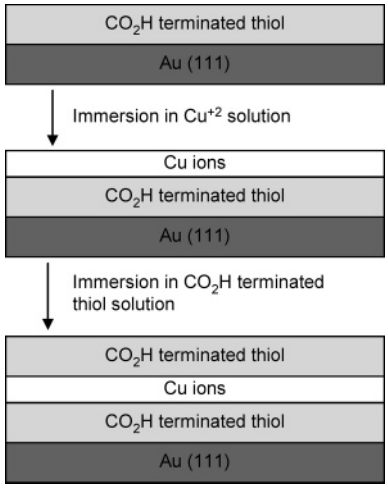

Figure 1. Schematic summarizing the formation of multilayers using the general method of Ulman and co-workers:[8] (1) formation of an α,ω-mercaptoalkanioc acid/Au SAM; (2) coordination of neighboring CO_2H terminal groups with Cu^{2+} ions; (3) formation of an overlayer of α,ω-mercaptoalkanoic acid molecules via RSH−Cu interaction. Steps 2 and 3 are repeated to build the stack layer by layer.

of the thickness and surface roughness of the MRFs as well as the interfacial topography and adhesive interaction of the deposited metal overlayer with the molecular films. In this regard, the growth of the α,ω-mercaptoalkanoic acid/Cu^{2+} MRFs can be problematic. For example, recent work has shown that while <10 nm junctions can be fabricated with MRF lift-off processing, poor reproducibility in the electronic characteristics of the resulting structures limits the quality of the information obtainable.[5] In similar work by Weiss and co-workers,[4] the rate of successfully nanofabricated separation using multilayer lithographic techniques decreased as the area of the interface increased.

To reliably control the final feature characteristics, it is clear that one needs to understand the details of the multilayer growth mechanisms and intermediate layer structures. In the case of the mercaptoalkanoic acid/Cu^{2+} strategy critical details are lacking. With respect to the interlayer structures and chemistry, the work of Ulman and co-workers provided few details about the interlayer binding chemistry and molecular packing structures.[9] In a subsequent study, Bard and co-workers[10] determined that the self-assembly of an α,ω-mercaptoalkanoic acid layer on a $-CO_2H$-terminated surface, previously coordinated with Cu^{2+} ions, leads to reduction of the metal to the Cu^{1+} state, but details of the actual molecular structures, coverages, and packing were not provided.

Given our long-term interest in producing highly precise gaps and features for building molecular electronics devices and other applications, it was of interest to study critical details of MRF structures and their growth mechanisms. Since the mercaptoalkanoic acid/Cu^{2+} films are currently the "standard" system, we focused our initial efforts on these films. In this study we address the nature of the interfacial layers and the chemical reactions that govern them by use of infrared reflection spectroscopy (IRS), X-ray photoelectron spectroscopy (XPS), single-wavelength ellispsometry (SWE), and atomic force microscopy (AFM). The study was done in three parts. First, we characterized the interfacial properties of a simple bilayer film built from adsorption of hexadecanethiol [$CH_3(CH_2)_{15}SH$] molecules and their deuterated analogues onto the Cu^{2+}-coordinated surface of $-CO_2H$-terminated SAMs formed from 16-mercaptohexadecanoic SAMs on Au{111} [$HO_2C(CH_2)_{15}S-$/Au], wherein the only interaction of the adlayer with the foundation SAM can be with the SH group. This simplified model system was limited intentionally to isolate the first interfacial layer. Second, we used 16-mercaptohexadecanoic acid [$CO_2H(CH_2)_{15}SH$] to form the adlayer and studied the effects of the carboxylic acid group on the bilayer formation. Finally, we used a $-CO_2H$-terminated SAM formed from 15-mercaptopentadecanoic acid [CO_2H-$(CH_2)_{14}S-$/Au] to determine whether any odd−even alkane chain length variation affects critical features of the multilayer films.[11,18−20] The overall results of these experiments show that stacks are bound by ligation to Cu(I) species with a resultant stoichiometry that drives the adlayers to coverages approaching ∼50% of that of the foundation SAM and further imparts a roughened molecular topography due to island formation. Some recovery of the coverages can be obtained by backfilling procedures, but recovery of the full value of the foundation SAM was not achieved in our hands. These results provide a significant advance in the understanding of the formation mechanism for this type of multilayer film and further demonstrate how this information can be used to advance the design of accurate spacer films for nanolithography in both fundamental research and technology applications.

2. Experimental Section

2.1. Materials. Copper(II) perchlorate hexahydrate [$Cu(ClO_4)_2 \cdot 6H_2O$] (98%, Aldrich), hexadecanethiol [$CH_3(CH_2)_{15}SH$] (95%, Fluka), hydrochloric acid (HCl) (38%, J. T. Baker), ethanol (neat, Pharmco), acetone (98% Aldrich), Milli-Q water (Millipore Products, Bedford, MA), and hexadecane (99.5%, Aldrich) were used as received. Hexadecanethiol (MH) [$CH_3(CH_2)_{15}SH$] (95%, Fluka) and 16-Mercaptohexadecanoic acid (MHA) (90%, Aldrich) were recrystallized before use. Deuterated hexadecanethiol ($CD_3(CH_2)_{15}$-SH) and 15-mercaptopentadecanoic acid (MPA) were synthesized as previously described.[21]

2.2. Sample Preparation. The metal films were deposited on silicon substrates (with a native oxide) which were first cleaned with a H_2O_2/H_2SO_4 solution,[22] rinsed with water and ethanol, and finally blown dry with N_2. The metal films were prepared via vapor deposition of a ∼10 nm thick Cr adhesion layer followed immediately by a ∼200 nm thick Au layer deposited using a resistively heated boat (pressure maintained continuously at $\sim 10^{-8}$ Torr during both depositions.) The Au/Cr/SiO_2/Si films typically showed roughness RMS values of 1.2 ± 0.2 nm by tapping mode AFM with most values at the lower end of the range. The freshly evaporated substrates were removed from the deposition chamber, immediately characterized by single-wavelength ellipsometry (several spots on each sample), and then placed into the monolayer solution. The total time for this sequence was within ∼5 min.

The multilayer films were prepared in the following sequential manner: (1) immersion of the Au substrate in a ∼1 mM ethanol solution of the MHA or MPA for a preselected time in the range of 2−24 h; (2) removal of the sample, rinsing in ethanol, followed by 0.02 M HCl in ethanol (concentrated aqueous HCl diluted in ethanol) and finally pure ethanol; (3) immersion in a ∼5 mM solution of $Cu^{II}(ClO_4)_2$ in ethanol for varying times of up to 3 min, removal, and thorough washing with neat ethanol;[23] (4) immersion in a ∼5 mM MH ($C_{16}D_{33}SH$ for the IRS samples and MHA or MPA for trilayer samples) solution in ethanol for varying times from 10 min

(18) Nishi, N.; Hobara, D.; Yamamoto, M.; Kakiuchi, T. *J. Chem. Phys.* **2003**, *118* (4), 1904−1911.
(19) Azzam, W.; Cyganik, P.; Witte, G.; Buck, M.; Woll, C. *Langmuir* **2003**, *19* (20), 8262−8270.
(20) Lin, S. Y.; Tsai, T. K.; Lin, C. M.; Chen, C. H.; Chan, Y. C.; Chen, H. W. *Langmuir* **2002**, *18* (14), 5473−5478.
(21) Bain, C. D. Ph.D. Thesis, Harvard University, 1988.
(22) Stapleton, J. J.; Harder, P.; Daniel, T. A.; Reinard, M. D.; Yao, Y. X.; Price, D. W.; Tour, J. M.; Allara, D. L. *Langmuir* **2003**, *19* (20), 8245−8255.
(23) Thorough rinsing of the samples after the $Cu(ClO_4)_2$ is added was found to be a critical step since unremoved Cu ions can result in additional binding of admolecules in the form of Cu−thiol clusters at the surface, which leads to highly irreproducible results.

to 24 h, followed by rinsing in ethanol and drying in a N_2 stream. In some cases the final samples were cycled through steps 3 and 4 multiple times. All solutions were made and stored in screw-top fluoroware containers. Prior to sample analysis all samples were rinsed with ethanol and blown dry with N_2. All analyses were started within 15 min of removal from solution. For each processing sequence SWE and IRS analyses were done at each step.

2.3. Characterization Methods. *2.3.1. Single-Wavelength Ellipsometry*. Measurements were recorded using a Stokes ellipsometer (LSE Stokes ellipsometer, Gaertner Scientific Corp., Skokie, IL) set at 632.8 nm and a 70° angle of incidence. The thickness was based on an isotropic film model for the alkanethiol layers with *n*, the real part of the complex refractive index, set to 1.5 and *k*, the imaginary (loss) part, set to zero.[24] More rigorous anisotropic models[25] were not considered because of the complexity of the layered structures. For a fully adsorbed Cu^{2+} layer on the SAM surface, *n* and *k* were set to 2.0 and 0.0.[26] In all cases, measurements were taken on at least three separate points on each sample and the calculated thicknesses then averaged together.

2.3.2. Infrared Reflection Spectroscopy. Analyses were collected using a custom, in-house-modified FTIR spectrometer (FTS-7000, DigiLab, Randolph, MA) with an optical setup described in detail elsewhere.[27] The spectrometer and external optics were purged with CO_2 and H_2O-scrubbed air to minimize spectral interferences from these gases. All spectra were taken at an 86° angle of incidence with p-polarized light, and the instrument resolution was set to 2 cm^{-1}. Reflection spectral intensities are reported as $-[\log(R/R_0)]$, where R is the power reflectivity of the IR beam and R_0 is the reflectivity of a reference sample. R_0 is the spectrum of a $C_{16}D_{33}-S-$/Au{111} SAM or a $C_{16}H_{33}S-$/Au{111} SAM depending on the specific spectral region of interest for the sample.

Quantitative IRS in conjunction with theoretical simulations was used to determine the average molecular tilt (θ) and twist (ψ) angles of the molecules in the SAMs (Figure 2). The analyses have been previously reported[22,27] but are briefly summarized for reference. The vibrational modes utilized in the orientation analysis and their associated transition dipole directions are based on literature assignments.[27−33] Quantitative transmission spectra of a pure compound dispersed in KBr were used to generate optical function spectra [n, $k(\nu)$].[27] Using these data and standard algorithms,[27] sets of simulated anisotropic monolayer spectra were generated for varying molecular tilt and twist angles at selected thicknesses of the film of spectral interest.

2.3.3. X-ray Photoelectron Spectroscopy. Analyses were performed on a monochromatic Al Kα source instrument (Kratos, Axis Ultra, England) operating at 14 kV and 20 mA for an X-ray power of 280 W. Spectra were collected with a photoelectron takeoff angle of 90° from the sample surface plane, energy steps of 0.15 eV, and a pass energy of 40 eV for all atoms except for sulfur, for which a pass energy of 20 eV was used.[34] Spectra were taken sequentially over at least seven different spots for sufficiently short intervals to avoid reduction of the Cu^{2+} ions by secondary electron emission.[9,10,35] At least three different samples were run this way at each processing step with similar results for each obtained. For each type of sample, irradiation power−time studies were done to determine the damage characteristics of the analyses. All spectra were referenced to the Au $4f_{7/2}$ binding energy at 84.0 eV.

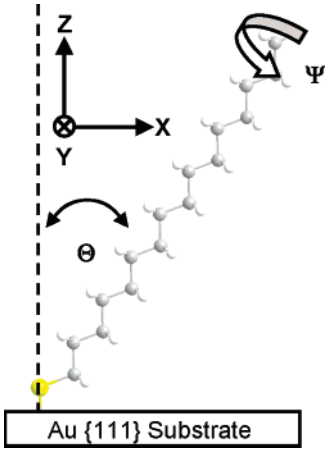

Figure 2. Definition of the tilt (θ) and twist (Ψ) angles of an alkanethiol molecule relative to the laboratory coordinate system, where the laboratory coordinate *Z* is perpendicular to the sample surface and the *xyz* molecular coordinate system is aligned with the laboratory *XYZ* system. The chains are initially aligned with the long axis in the *Z* direction and the C−C−C plane parallel to the *XZ* plane.

2.3.4. Contact Angles. Advancing and receding contact angles were measured using a home-built video-interfaced apparatus. All measurements were made with the sample at ambient conditions. A 20 μL drop of the probe liquid was dispensed onto the surface using a flat-tipped micrometer syringe (GS-1200, Gilmont Instruments, Barrington, IL). The advancing contact angle was measured as the drop expanded. The drop was then partially retracted into the syringe and the receding angle measured. Images of the drop were captured digitally using a CCD camera, and contact angles were analyzed using ImageJ 1.32j software (National Institutes of Health). Measurements were made on at least three separate spots for each sample with four samples taken for each processing step. Milli-Q water and hexadecane were used as probe liquids. In the case of hexadecane all contact angles were always less than 15°.

2.3.5. Atomic Force Microscopy. Tapping mode AFM images were taken using a Dimension Series 3100 (Digital Instruments, Santa Barbara, CA) scanning probe microscope using etched silicon tips (Nanosensors, NCH type, Neuchatel, Switzerland) with typical resonant frequencies between 270 and 330 kHz. To get substrates as flat as possible, the surfaces were prepared on Au(111) substrates on mica (Agilent/Molecular Imaging, Tempe, AZ) which were H_2 flame annealed immediately prior to monolayer formation.

3. Results and Discussion

For convenience the various stages of the film stack formation are labeled with reference designations, as summarized in Table 1. For stacks utilizing MPA as the starting SAM the symbols are designated with a "prime".

3.1. MHA|MH Bilayer Films. *3.1.1. Formation of the MHA SAM (A)*. The first step in the formation of multilayer structures is the formation of a clean, densely packed monolayer of a $-CO_2H$-terminated SAM. The initial SAMs were characterized

(24) Shi, J.; Hong, B.; Parikh, A. N.; Collins, R. W.; Allara, D. L. *Chem. Phys. Lett.* **1995**, *246* (1−2), 90−94. Given that other approximations were required, e.g., the refractive index of the Cu−SAM interfaces (see refs 25 and 26), the use of an isotropic chain model, as opposed to a more accurate anisotropic chain model, seemed appropriate.

(25) Parikh, A. N.; Allara, D. L. Effects of Optical Anisotropy on Spectro-Ellipsometric Data for Thin Films and Surfaces. In *Optical Studies on Real Surfaces and Inhomogeneous Thin Films*; Francombe, M., Ed.; Physics of Thin Films Series; Academic Press: New York, 1994; Vol. 19, pp 279−323.

(26) As no refractive indexes at 632.8 nm were available for the type of Cu^{2+} species that would be present in the carboxylate surface layer, the average refractive indexes of different simple copper salts was used to provide an estimate of an average value: atacamite ($Cu_2(OH)_3Cl$), ∼1.9; azurite ($Cu_3(OH)_2(CO_3)_2$), ∼1.8; malachite ($Cu_2(OH)_2(CO_3)$), ∼1.8; marshite (CuI), ∼2.3; nantokite (CuCl), ∼1.9.

(27) Parikh, A. N.; Allara, D. L. *J. Chem. Phys.* **1992**, *96* (2), 927−945.

(28) Socrates, G. *Infrared and Raman Characteristic Group Frequencies*; John Wiley & Sons, Ltd.: Chichester, U.K., 2001.

(29) Laibinis, P. E.; Nuzzo, R. G.; Whitesides, G. M. *J. Phys. Chem.* **1992**, *96*, 5097−5105

(30) Xu, C. J.; Sun, L.; Kepley, L. J.; Crooks, R. M.; Ricco, A. J. *Anal. Chem.* **1993**, *65*, 2102−2107.

(31) Snyder, R. G.; Strauss, H. L.; Elllger C. A. *J. Phys. Chem.* **1982**, *86*, 5145−5150.

(32) Snyder, R. G.; S. L. Hsu S. L.; Krimm S. *Spectrochim. Acta, A* **1978**, *34*, 395−406.

(33) Arnold R.; Azzam W.; Terfort A.; Woll C. *Langmuir* **2002**, *18*, 3980−3992

(34) Moulder J. F., Ed.; *Handbook of X-ray photoelectron spectroscopy*; Perkin-Elmer Corp.: Eden Prairie, MN, 1992.

(35) Knotek, M. L.; Feibelman, P. J. *Surf. Sci.* **1979**, *90* (1), 78−90.

Table 1. Summary and Designation of Samples for Each Step in the Multilayer Film Growth Process Starting with the MHA SAM, Labeled MHA[a]

no. of alkyl layers	starting sample and treatment	designation	short notation
1	MHA	MHA	A
1	MHA + Cu^{2+}	MHA−Cu	B
2	MHA−Cu + MH	MHA|MH	C
2	MHA|MH + Cu^{2+}	MHA|MH−Cu	D
2	MHA|MH−Cu + MH	MHA|MH (dense)	E
2	MHA−Cu + MHA	MHA|MHA	F
2	MHA|MHA + Cu^{2+}	MHA|MHA−Cu	G
3	MHA|MHA−Cu + MH	MHA|MHA|MH	H
3	MHA|MHA|MH−Cu + MH	MHA|MHA|MH (dense)	J

[a] The step designations also apply to mercaptopentadecanoic acid SAMs (MPA), but in the text the letters are designated with a prime (e.g., A′).

Table 2. Approximate Observed Frequencies for Selected Modes Assigned to Features in the Reflection Infrared Spectra of SAMs Formed from Chemisorption of Alkanethiols and Mercaptoalkanoic Acids on Au{111}[a]

frequency, cm^{-1}	mode assignment
3300−2500	general O−H stretches (ν_{OH})
2918	$-CH_2-$, antisym C−H stretch (d^-)
2850	$-CH_2-$, sym C−H stretch (d^+)
2700−2500	$-CO_2H$, O−H stretch ($\nu_{OH(CO_2H)}$)
2220	$-CD_3$, asym C−D stretch (r_a^-)
2194	$-CD_2-$, antisym C−D stretch (d^-)
2156	$-CD_3$, asym C−D stretch (r_b^-)
2090	$-CD_2-$, antisym C−D stretch (d^+)
2073	$-CD_3$, sym C−D stretch (r^+)
1741	$-CO_2H$ (free), C═O stretch ($\nu_{C=O}$)
1718	$-CO_2H$ (H-bonded), C═O stretch ($\nu_{C=O(H)}$)
1695−1540	$-CO_2^-$, antisym C═O stretch ($\nu_{a(CO_2^-)}$)
1450−1335	$-CO_2^-$, sym C═O stretch ($\nu_{s(CO_2^-)}$)
1471	$-CH_2-$, main chain scissor deformation (δ)
1412	$-CH_2-$, α-CH_2 scissor deformation in $-(CH_2)_nCO_2H$ (δ_α)
1170−1040	ClO_4^-, antisym stretch ($\nu_{a(ClO_4^-)}$)
955−930	ClO_4^-, sym stretch ($\nu_{s(ClO_4^-)}$)

[a] Mode assignments were made on the basis of previous reports (for details see the text).

via IR, XPS, SWE, and contact angle measurements to verify the structure and determine the cleanliness of the surfaces. Detailed characterization of the relevant IR modes have been presented in detail elsewhere[27−33] and are summarized for convenience in Table 2. The C−H stretching mode spectrum in Figure 3 (labeled MHA and A) shows the d^+ and d^- modes at 2851 and 2919 cm^{-1}, respectively. Comparison of simulated (dotted line for MHA/A) and experimental spectra yielded the best fit for an all-trans structure with an average chain tilt (θ) and twist (ψ) of 33 ± 3 and 52 ± 3°, respectively,[36] in agreement with previous work.[7] In the lower frequency region (Figure 4, spectrum A) the doublet at 1742 and 1717 cm^{-1} is due to the C═O stretches ($\nu_{C=O}$) of the free and H-bonded carboxylic acid species, respectively. The CH_2 scissor modes (γ_{CH_2}) appear at 1469 and 1411 cm^{-1}, for the main chain and α-C methylenes, respectively.[7] We find that a critical step in the formation of reproducible multilayer stack results is thorough removal of adventitious contamination (e.g., fatty acids from laboratory air) on the initial CO_2H SAM, typically by rinsing with dilute (ethanol) HCl solution. In previous work, extended (24 h) exposure to HCl solution was found to cause some esterfication of the MHDA.[33] In this work, no evidence of esterfication was observed after the brief HCl rinse. Once the sample is cleaned, the $\nu_{C=O}$ IR modes are consistently as shown in Figure 4 and the advancing and

(36) The thicknesses for all simulations are based on the SWE measurements taken for each film. A refractive index of 1.48 was used for the organic layers.

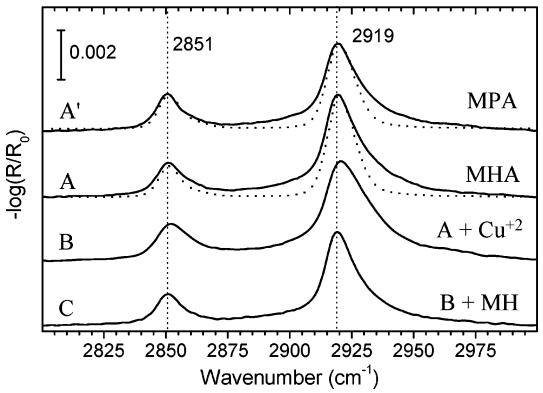

Figure 3. Infrared spectra of the C−H stretching modes for stages A−C of bilayer film growth. The dotted lines represent the best fit simulation spectra which give average chain tilts/twists of 33 ± 3°/52 ± 3° and 32 ± 3°/49 ± 3°, respectively, for the MHA and MPA SAMs. Addition of Cu^{2+} ions (B) causes slight disordering of the alkyl chains, observed as a +2 cm^{-1} shift in both the d^+ and d^- modes relative to the bare monolayer (A). The addition of a thiol adlayer causes a shift back to the original frequency (C).

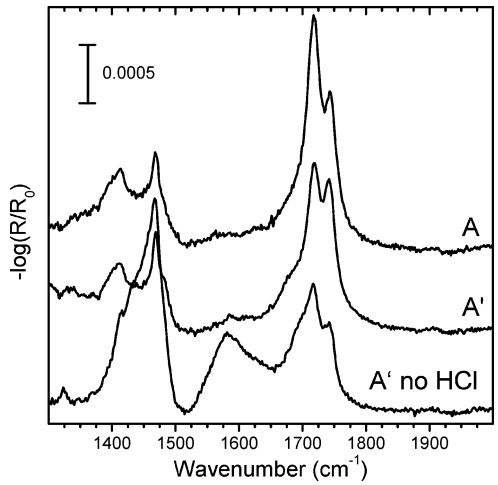

Figure 4. Infrared spectra of the C═O stretching mode region for an MHA SAM (A) and an MPA SAM (A′) showing the $\nu_{C=O}$ feature for H-bonded (~1718 cm^{-1}) and free (~1741 cm^{-1}) CO_2H groups. The bottom spectrum (A′**,** no HCl) is a typical example of an MPA SAM which has not been surface cleaned to remove contaminants.

receding H_2O contact angles minimize to <10° (Table 3).[8,9,37] Further, in our hands, the best multilayer stacks resulted when the CO_2H SAM was formed with at least 12−24 h of incubation.[38]

3.1.2. Formation of the MPA SAM (A′). Odd−Even Chain Effects. To explore odd−even chain length effects,[18−20] SAMs of MPA were also used. The thickness and wetting characteristics of the MPA and MHA SAMs were observed to be nearly identical within error (Table 3). The C−H stretching region IR features appear at identical frequencies (Figure 3), a measure of nearly identical alkyl chain conformational ordering and orientation. An ideal all-trans structure forces different orientations of the CO_2H terminal group for the two SAMs, as suggested by the simple stick structures shown in Figure 5. A manifestation of this is observed by the reproducibly different intensity ratios of

(37) Whitesides G. M.; Laibinis P. E. *Langmuir* **1990**, *6*, 87−96.

(38) This period gave minimum frequency positions of the d^+ and d^- modes (indicating a maximum point of the degree of conformational ordering) and good surface cleanliness. Longer times showed constant conformational ordering but resulted in increasing surface contamination, likely in part from the formation of surface dimers by physisorption of solute MHA molecules to the surface CO_2H groups.

Table 3. Thickness and Contact Angle Measurements for Bilayers of MHA|MH (A−E) and MPA|MH (A′−E′) for Each Step of Their Respective MH Bilayer Growth[a]

	SWE measurements, Å		H_2O contact angle (θ_{H_2O}), deg	
sample	thickness (d)	$d_{sample} - d_A$	θ(adv)	θ(rec)
A	20 ± 1	0	<10	<10
B	21 ± 1	1	22 ± 3	<10
C	39 ± 1	18	83 ± 7	33 ± 4
D	34 ± 1	14	72 ± 9	27 ± 3
E	42 ± 1	22	84 ± 2	37 ± 3
F	36 ± 1	16	NA	NA
H	48 ± 2	28	NA	NA
J	56 ± 2	36	NA	NA

	SWE measurements, Å		H_2O contact angle (θ_{H_2O}), deg	
sample	thickness (d)	$d_{sample} - d_{A'}$	θ(adv)	θ(rec)
A′	19 ± 1	0	<10	<10
B′	20 ± 1	1	21 ± 6	<10
C′	39 ± 2	19	84 ± 7	25 ± 5
D′	35 ± 2	16	62 ± 4	<15
E′	42 ± 3	23	83 ± 7	35 ± 9

[a] NA = not available.

the $\nu_{C=O(H)}$ and $\nu_{C=O}$ features (1718 and 1741 cm^{-1}, respectively, in Figure 4), which show a greater contribution of the H-bonded C═O species in the MHA (C16) SAM. While both monolayers showed maximum organization after ∼24 h deposition times (minimum d^- peak frequencies), the MPA SAMs typically showed much greater amounts of surface contamination for similar deposition times and ambient exposures.[39]

3.1.3. Immersion of the MHA SAM in $Cu(ClO_4)_2$ Solution Forms a Complete $Cu^{II}(CO_2^-)_2$ Surface (A → B). Placing the cleaned MHA SAMs in 5 mM $Cu^{II}(ClO_4)_2$ solution in ethanol for varying times (5−180 s) shows complete coordination within ∼30 s,[23] by all measurement techniques with no changes for longer times. The SWE thickness (Table 3) is ∼+1 Å thicker on average (modeling with $n \approx 2.0$ for a Cu^{2+} adlayer) than that of the starting SAM.[26] The disappearance of the $\nu_{C=O(H)}$ and $\nu_{C=O}$ modes and the appearance of the $\nu_{s(CO_2^-)}$ and $\nu_{a(CO_2^-)}$ modes (1444 and 1603 cm^{-1}, respectively) in the IR spectra (compare spectra A and B in Figure 6) show near-exhaustive conversion of the CO_2H groups to carboxylate species. The absence of the intrinsically intense ClO_4^- stretch mode features (945 and 1100 cm^{-1}) and no observable Cl 2p XPS core level signal (data not shown) show the absence of this ion. The O 1s XPS spectrum (Figure 7) shifts from the initial doublet (532.6 and 534.0 eV) of the CO_2H group[40] to a singlet at 531.8 eV, appropriate for a symmetrical CO_2^- species (compare spectra A and B in Figure 7). Though the Cu $2p_{3/2}$ region shows the appearance of both the Cu(II) (934.7 eV with shake-up peaks at 940 and 944 eV) and Cu(I) (932.8 eV) oxidation states (Figure 7), the Cu(I) feature is found to increase in intensity with increased beam exposure and so is considered an artifact.[9,10] The C 1s spectrum shows a shift of both the $-CH_2-$ and $-CO_2H$ peaks to lower binding energies (Figure 7), consistent with formation of a surface carboxylate anion,[41,42] and the S 2p spectrum shows no change (compare spectra A and B in Figure 7) with component peaks

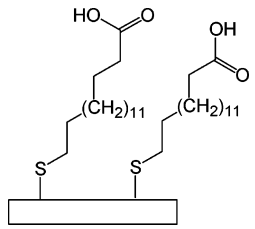

Figure 5. Idealized planar all-trans chain structures for odd and even mercaptoalkanoic acid SAM molecules on Au{111}. The structures are meant to convey only the placement of the terminal groups relative to the substrate bonding geometry and cannot convey the actual distribution of conformations expected in a given SAM.

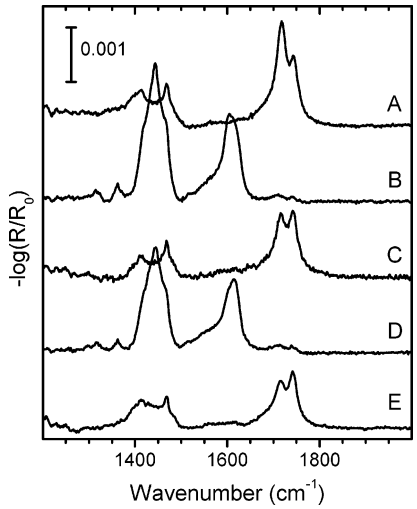

Figure 6. Infrared spectra of the low-frequency region for stages A−E of growth for a bilayer film.

remaining at 161.9 and 163.1 eV, in agreement with the reported positions for alkanethiolate/Au SAMs.[43]

All of these data are consistent with the surface reaction

$$2RCO_2H(s) + Cu^{2+}(aq) \rightarrow (RCO_2^-)_2Cu^{2+}(s) + 2H^+(aq) \quad (1)$$

where R = $-S(CH_2)_{15}-$, aq = aqueous, and s = surface. Consistent with the ligation of each Cu^{2+} ion to a pair of adjacent $-CO_2^-$ terminal groups, a decrease in the chain conformational ordering is observed as indicated by the +2 cm^{-1} shift in the d^- mode (Figure 3). This slight disordering appears to be caused by the steric requirements for ligation of a pair of adjacent CO_2^- groups to one Cu^{2+} ion (a more detailed discussion will be given in section 3.2.3).

3.1.4. Formation of the MHA|MH Bilayer Results in Reduction of Cu(II) to Cu(I) and a Limiting 50% Coverage MH Adlayer (B → C). The MHA−Cu samples were placed in ∼5 mM MH solutions in ethanol for varying times ranging from 10 min to 24 h. Optimum times are ∼30 min, and this time is used for all the experiments reported here.[44] The MHA−Cu → MHA|MH conversion results in a ∼18 Å increase in the SWE thickness (to ∼39 ± 1 Å) and a final θ_{H_2O}(adv) = 83 ± 7° with $\Delta\theta$ = 50° (see Table 3). In comparison with a bare MH SAM ($\Delta\theta$ = 8°), the 50° wetting hysteresis suggests a much lower adlayer packing density with a higher number of surface defects.[45,46]

The main features of the adlayer interface chemistry can be seen readily in the XPS spectra (Figure 7). The main observations

(39) We note that, relative to the MHA SAMs, the MPA SAMs needed to be cleaned much more thoroughly to produce a constant surface and were more difficult to keep clean.

(40) Konstadinidis, K.; Zhang, P.; Opila, R. L.; Allara, D. L. *Surf. Sci.* **1995**, *338*, 300−312.

(41) The bare MHA monolayer shows $-CH_2-$ and $-CO_2H$ C 1s peaks at 284.7 and 289.4 eV, respectively. Addition of copper ions (Figure 7B) causes respective shifts of −0.9 and −0.3 eV. These types of shifts have been noted for similar surfaces and have been attributed to surface charging (see refs 8, 9, and 42).

(42) For general information on charging effects observed in XPS see: Briggs, D.; Grant J. T. Surface *Analysis by Auger and X-Ray Photoelectron Spectroscopy*; IM Publications and Surface S pectra Ltd.: West Sussex, U.K., 2003.

(43) Duwez, A. S. *J. Electron Spectrosc. Relat. Phenom.* **2004**, *134* (2−3), 97−138.

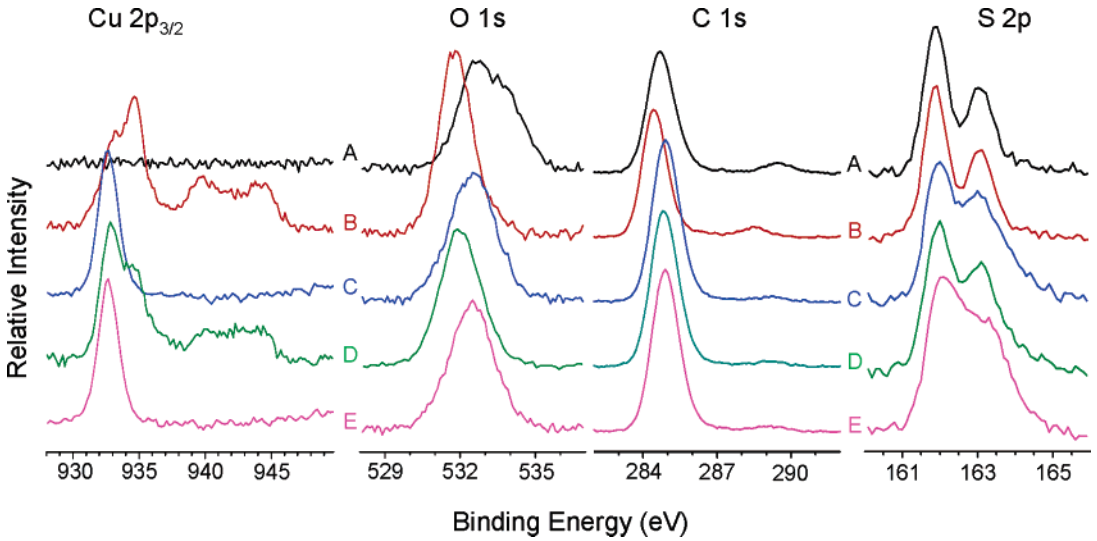

Figure 7. XPS Cu $2p_{3/2}$, O 1s, C 1s, and S 2p spectra for growth stages A−E.

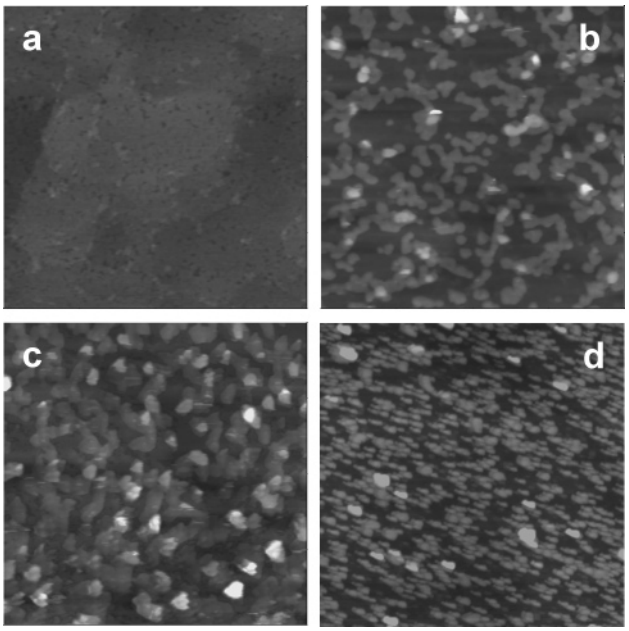

Figure 8. Tapping mode AFM images (1 μm^2; all images have a 20 nm height scale): (a) clean MHA surface (A) (note the clear appearance of the underlying step edges of the Au substrate; the scattered lighter features are attributed to the presence of dimers formed by H-bonding of solute MHA molecules to surface CO_2H sites of the MHA SAM); (b) after addition of an MH adlayer to the MHA surface (A → C); (c) after densification of the initially formed MHA|MH surface (C → E); (d) after addition of an MHA adlayer to the MHA surface (A → F). Images comparing MHA (A) to MHA|Cu_2^+ (B) surfaces show no significant observable differences.

upon formation of the adlayer (B → C) are (1) the O 1s spectrum changes from a sharp 531.8 eV feature to a relatively broad one at 532.5 eV with apparent components from both CO_2H and CO_2^- species, (2) the C 1s, $-CO_2H$ feature shifts to a broad peak (288.9 eV) consistent with both $-CO_2H$ and CO_2^- species components at 289.4 and 288.5 eV,[47](3) only a single 932.8 eV

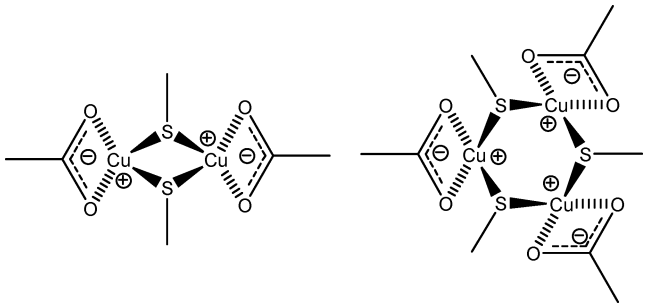

Figure 9. Possible Cu(I)−S bridging structures found on the surface.

Cu $2p_{3/2}$ peak is observed accompanied by a Cu LMM Auger line at 916 eV (not shown), indicative of formation of a Cu(I) species,[10,34]and (4) the S 2p spectrum changes dramatically from a doublet to a single peak with a line shape consistent with Au−*S*−CH_2− and Cu−*S*−CH_2− components (161.9 ± 0.1 and 162.4 ± 0.1 eV, respectively).[48]

Pursuing the last observation further, by peak fitting[49] and accounting for photoelectron mean free path effects,[43,50,51] the MHA|MH S 2p spectrum gives a (0.4 ± 0.1):1 (Cu−*S*R):(Au−*S*R′) ratio. This ratio is consistent with a ∼50% MH adlayer coverage with a ∼1:1 Cu(I):[$-S(CH_2)_{15}CH_3$] ratio and leads to the reaction stoichiometry in eq 2, where R and s are defined as in eq 1, soln = ethanol solution, and R′ = $-(CH_2)_{15}CH_3$.

$$(RCO_2^-)_2Cu^{2+}(s) + HSR'(soln) \rightarrow [RCO_2^-Cu^+]SR'(s) + RCO_2H(s) \quad (2)$$

Consistent with this reaction, the low-frequency IR (Figure 6, spectrum C) shows the $\nu_{a(CO_2^-)}$ and $\nu_{s(CO_2^-)}$ peaks vanish while the $-CO_2H$ features reappear, though not as intense as in the bare

(44) Experiments with deuterated MH show that the MH molecules increasingly begin inserting into the MHA underlayer for increasingly longer solution deposition periods above 30 min. This process in turn reduces the number of copper coordination sites and eventually leads to poorly structured bilayers. To minimize insertion, very short solution depositions are needed with 30 min optimum for completely reducing the Cu(II) while avoiding interlayer exchange.

(45) Bain, C. D.; Troughton, E. B.; Tao, Y. T.; Evall, J.; Whitesides, G. M.; Nuzzo, R. G. *J. Am. Chem. Soc.* **1989**, *111*, 321−335.

(46) Note that previous studies report θ_{H_2O}(adv) ≈ 95° and 103° for $-(CH_2)_{17}-CH_3$ chains grafted with ∼50% molecularly uniform coverages across planar surfaces [Parikh, A. N.; Liedberg, B.; Atre, S. V.; Ho, M.; Allara, D. L. *J. Am. Chem. Soc.* **1995**, *99* (24), 9996−10008. Allara, D. L.; Parikh, A. N.; Judge, E. *J. Chem. Phys*. **1994**, *100*, 1761−1764]. In comparison to the θ_{H_2O}(adv) ≈ 83° for the MHA|MH adlayer sample, these results suggest that the MH adlayer has a coverage of <50% and/or is not uniformly distributed, viz., is distributed as islands.

(47) The much lower relative intensity of the $-CO_2H$ component in the MHA|MH bilayer film compared to the MHA and MHA−Cu films is presumably due to photoelectron screening effects from the adlayer and to the increased number of $-CH_2$− units in the MHA|MH film.

(48) Laffineur, F.; Delhalle, J.; Guittard, S.; Geribaldi, S.; Mekhalif, Z. *Colloids Surf., A* **2002**, *198* 817−827.

MHA monolayer. Close inspection of the $\nu_{C=O}$ and $\nu_{C=O(H)}$ peaks reveals that the ratio of H-bonded to free $-CO_2H$ groups is reduced compared to that of the bare MHA SAM. This is consistent with a mixed CO_2^- and CO_2H bilayer interface in which the presence of the CO_2^- groups reduces the fraction of adjacent CO_2H groups.

Structural details of the alkyl chain structures in the bilayer were probed using $HS(CD_2)_{15}CD_3$ (DMH) to separate the IRS C−H modes for each layer. The d^+ and d^- mode C−D stretches for the MHA|(DMH) bilayer (Figure 8) occur at 2092 and 2194 cm^{-1}, respectively. These values are quite close to those for the DMH/Au SAM (2090 and 2194 cm^{-1})[52] and indicate that the adlayer chains exhibit a degree of conformational order similar to that in a typical hexadecanethiolate SAM on Au.[7] Given that the XPS data indicate a ∼50% surface density of chains in the adlayer compared to the MH SAM while the wetting data suggest highly nonuniform coverage, the IRS data drive the conclusion that the adlayer forms as islands or ensembles of highly organized chains.[53]

Tapping mode AFM images of the surface taken before and after the addition of MH reveal clear island growth structures (Figure 8). Attempts to quantitate important physical characteristics from the images unfortunately were difficult. The significant differences in the tip (silicon oxide)−surface interactions between the MHA underlayer (hydrophilic) and the MH islands (hydrophobic) complicated measurement of the island heights,[54] while tip-induced mobility of many of the islands complicated confirmation of the relative coverage determined from the S 2p XPS data.[55]

The island structure of the MH adlayer indicates that the admolecules suffer a driving force to pack in ensembles, as opposed to random attachment to the underlayer with consequent high chain disorder. One possible reason could be the propensity of Cu(I) to form bridging structures with thiol ligands,[56,57] for example, as shown in Figure 9. In the actual bilayer interface more complicated bridging structures would be likely.

Finally, note that the MHA underlayer d^+ and d^- mode C−H stretches (Figure 3, spectrum C) are located at 2851 and 2919 cm^{-1}, respectively, the original position of the starting MHA SAM before addition of $Cu(ClO_4)_2$ and ∼−2 cm^{-1} shifted from that the MHA−Cu structure. Thus, the formation of the adlayer (eq 2) eliminates the MHA layer chain disordering caused by ligation of Cu^{2+} ions (eq 1), presumably by the release of the constraint of adjacent $-CO_2^-$ terminal group pairing to a single Cu^{2+} counterion that occurs when Cu^{2+} is reduced to Cu^{1+}.

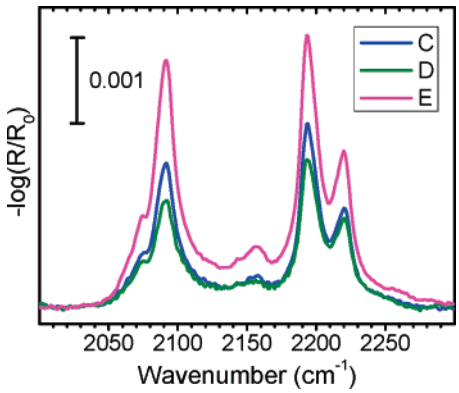

Figure 10. Infrared spectra of the C−D stretching modes for the C−E stages of growth of a bilayer film.

3.1.5. Densification of the MHA|MH Bilayer by Sequential Readdition of $Cu(ClO_4)_2$ and MH. 3.1.5.1. Addition of Cu^{2+} to the MHA|MH Bilayer Film To Form MHA|MH−Cu (C → D). Since the initially formed MHA|MH bilayer interface has ∼50% coverage of $-CO_2H$ groups, a method utilizing sequential readdition of Cu^{2+} and MH molecules was explored to attach additional adlayer molecules to these groups and thereby densify the adlayer with filling in of the MH island structure. To start, the initially formed bilayer samples were immersed in 5 mM $Cu(ClO_4)_2$ solution in ethanol for varying times from 5 to 180 s. The optimum time was found to be ∼30 s, and this time is used for all the results reported here, unless otherwise stated.

Both the XPS and IRS data demonstrate near-quantitative ligation of Cu^{2+} ions to the remaining $-CO_2H$ groups after the Cu^{2+} reimmersion step. After initial addition of $Cu(ClO_4)_2$ XPS (Figure 7, spectrum D) shows a sharpening of the O 1s peak with a shift to 532.0 eV and a shift of the $Cu_{2p\ 3/2}$ peak from the Cu(I) value (932.8 eV for the initial MHA|MH bilayer) to a value appropriate for a mixture of Cu(I) and Cu(II) (934.7 eV with satellite peaks at 940 and 944 eV). These data are all consistent with formation of $-CO_2^-$ species (see section 3.1.4). In agreement, the IRS data (Figure 6, spectrum D) show a near-complete loss of the $-CO_2H$ C=O stretching mode features,[58] while the corresponding $-CO_2^-$ modes gain in intensity.

The overall process, however, is more complicated than a simple ligation of Cu^{2+} ions to $-CO_2H$ groups. A decrease in film integrity is indicated by an overall loss of material indicated by a ∼5 Å decrease in the SWE film thickness (Table 3), a ∼11° decrease in the H_2O contact angle (Table 3), and a decrease in the C 1s XPS signal. This loss is predominately in the adlayer indicated by a loss of intensity of the C−D MH adlayer IRS stretching modes (Figure 10, spectrum D) with little change in the corresponding MH underlayer C−H intensities. The S 2p XPS spectra are consistent with this conclusion as shown by an experiment run with 2 min of immersion (rather than the standard 30 s) to drive the adlayer loss to a larger extent. After immersion,

(49) The S 2p peaks were constrained similarly to have a self-consistent comparison. The area of the $S_{2p_{1/2}}$ electrons was set to $^1/_2$ that of the $S_{2p_{3/2}}$ electrons, the positions of the $S_{2p_{1/2}}$ electrons were fixed to be 1.2 eV higher than those of the $S_{2p_{3/2}}$ electrons, and the positions of the $S_{2p_{3/2}}$ electrons were fixed to the literature values of 161.9 for Au−S, 162.4 for Cu−S, and 163.5 for S−H (free thiol). The full widths at half-maximum (fwhm's) were allowed to range from 0.8 to 1.0 eV, based upon the fwhm of the MHA SAM spectrum, and the fwhm's of all the peaks were fixed equal to each other.

(50) Jablonski, A.; Powell, C. J. *Surf. Sci. Rep.* **2002**, *47* (2−3), 35−91.

(51) To calculate the relative intensity, it is necessary to first take into account the depth of the samples and how much the signal is attenuated. The intensity of each sulfur atom was adjusted using the following equation: $I(S) = I_0(S)\, e^{-d/(\lambda \sin \theta)}$, where $I(S)$ is the intensity from the gold photoelectrons attenuated by the monolayer, $I_0(S)$ is the intensity of a clean sulfur substrate, d is the depth, θ is the takeoff angle (90°), and λ is the photoelectron mean free path (3.6 nm). By manipulating the equation, the ratio of S−Cu to S−Au can be found, $I_{S-Au}/I_{S-Cu} = e^{-\Delta d/\lambda}$, where Δd is the difference in the depth between the two sulfurs. For 16-mercaptohexadecanoic acid the ratio is $I_{S-Au}/I_{S-Cu} = 0.558$, and for 15-mercaptoheptadecanoic acid the ratio is $I_{S-Au}/I_{S-Cu} = 0.574$.

(52) The positions for the d^+ and d^- C−D modes for pure deuterated MH monolayers on Au were used as reference spectra.

(53) Simulations of a multilayered surface utilizing a Maxwell Garnett effective medium approximation combined with anisotropic chain structures (uniaxial symmetry) yielded generally poor fits. It is presumed that this is due primarily to the nonuniform distribution of orientations of MH molecules on the surface.

(54) Brandsch, R.; Bar, G.; Whangbo, M. H. *Langmuir* **1997**, *13* (24), 6349−6353.

(55) Contact mode AFM was found to be highly damaging to the surface caused by the tip interactions easily moving the adlayer islands around the surface. These effects could be significantly reduced by optimizing the tapping oscillation amplitudes.

(56) Espinet, P.; Lequerica, M. C.; Martin-Alvarez, J. M. *Chem.—Eur. J.* **1999**, *5* (7), 1982−1986.

(57) Holloway, C. E.; Melnik, M. *Rev. Inorg. Chem.* **1995**, *15* (3−4), 147−386.

(58) An average of 5% of the original intensity often remainsm and this reduced intensity does not significantly decrease with longer copper solution deposition times. The remaining signal is attributed to a small fraction of the reactive carboxylic acid sites at the interface being protected by hexadecanethiol molecules physically blocking the path to the acid group.

the reduction in the (Cu−*S*R):(Au−*S*R) intensity ratio from (0.4 ± 0.1):1 to (0.3 ± 0.1):1 indicates a loss of the adlayer thiol molecules (compare spectra C and D in Figure 7).

The data suggest that a parallel metathesis reaction occurs with incorporation of Cu^{2+} ions from solution into the bilayer and release of $Cu^{+}[S(CH_2)_{15}CH_3]$ ions into solution (with ClO_4^- counterions):

$$2[RCO_2^-Cu^+SR'(s) + RCO_2H(s)] + Cu^{2+}(aq) \rightarrow [(RCO_2^-)_2Cu^{2+}](s) + 2R'SCu^+(aq) \quad (3)$$

where the abbreviations are defined as in eq 2.

3.1.5.2. Readdition of MH to the MHA|MH−Cu Bilayer Film To Form the Densified MHA|MH(dense) Bilayer (D → E). Samples were then placed in ∼5 mM MH solutions (DMH for IR samples) in ethanol for varying times ranging from 10 min to 24 h. The results presented in this section are for the optimized time of 30 min.

After immersion the film incorporates admolecules as shown by an SWE thickness increase of ∼8 Å (to ∼42 ± 1 Å, Table 3) or ∼3 Å compared to the thickness of the initial bilayer film (MHA|MH, C). In agreement, the intensities of the IRS C−D stretching modes increase significantly relative to those of the original MHA|DMH bilayer (compare spectra D and E in Figure 10), while the (Cu−*S*R′):(Au−*S*R) S 2p XPS peak intensity ratio increases from (0.4 ± 0.1):1 to (0.7 ± 0.1):1 (compare spectra C and E in Figure 7).[59] These data indicate that the second sequential cycle of Cu^{2+} and MH addition densifies the initial MHA|MH adlayer by up to 75%. Note that the C−H d^+ and d^- stretch mode peak positions exhibit the same conformational ordering as for the original MHA|MH islanded bilayer (compare spectra C and E in Figure 10), so densification continues the same extent of chain ordering. Consistent with the incomplete coverage of the densified adlayer, the H_2O contact angle remains nearly the same as that of the original MHA|MH bilayer with only a slight decrease in hysteresis (Table 3).[60] Finally, AFM images (Figure 8c) confirm the densification and show a rough topography consistent with continued islanding of the adlayer molecules.

The associated interface chemistry follows the above observations. Similar to the original MH adlayer addition, the IRS data show a complete loss of $-CO_2^-$ mode intensities with a recovery of the $-CO_2H$ modes (compare spectra C−E in Figure 6). Note also the C═O stretching mode peaks indicate that the ratio of H-bonded to isolated $-CO_2H$ species shifts to a higher fraction of the isolated species relative to that of the initial MHA|MH bilayer (C) and the bare MHA SAM (A). The Cu $2p_{3/2}$ XPS region (Figure 7, spectrum E) shows a single peak at 932.8 eV, indicative of only a Cu(I) species. Overall, the reaction chemistry appears to be the same as in eqs 1 and 2 with one admolecule incorporated as a $[Cu^+]SR'$ species per two original $-CO_2H$ groups at the bilayer interface. Given the side exchange side reaction in eq 3, the incorporation of impurities with continued processing,[60] and the constraint of two adjacent $-CO_2H$ groups for the initial Cu^{2+} ligation step, it is clear that achievement of complete densification to a full MH adlayer is highly problematic. In our hands, we have found no advantage for continuing on after the second addition of the adlayer as either the surface coverage is similar to that of the second addition or continued deteriorations in film quality are observed.

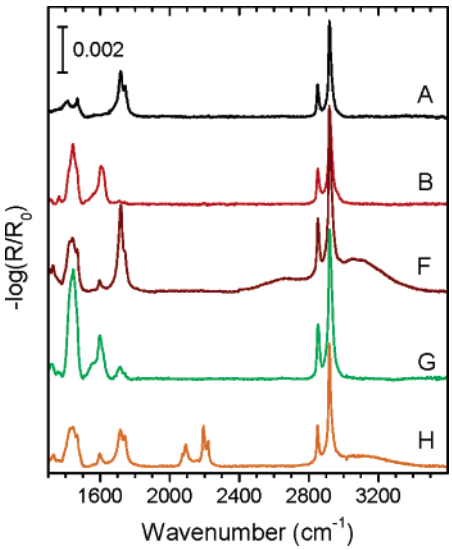

Figure 11. Infrared spectra for the five steps of growth of a trilayer film.

3.2. MHA|MHA|MH Trilayer Films (H). *3.2.1. Formation and Thickness of the MHA|MHA Bilayer (B → F).* The MHA−Cu surfaces (B) were placed in ∼5 mM MHA solutions in ethanol for varying times ranging from 10 min to 24 h. The results are given for our observed optimum time of ∼2 h. After immersion, the thickness increases by ∼15 Å to 36 ± 1 Å, slightly less than the thickness of the MHA|MH bilayer (∼39 Å, Table 3). Since the MHA molecule is slightly longer than the MH molecule when fully extended,[61] the adlayer coverage appears lower for the MHA|MHA bilayer than the MHA|MH bilayer. However, experimental results suggest similar coverages between the two adlayer systems with intermolecular interactions resulting in a lower thickness for the MHA|MHA bilayer.

3.2.1.1. The MHA Adlayers in MHA|MHA Bilayers (F) Exhibit Loosely Packed Alkyl Chains and Enhanced Intermolecular H-Bonding at Terminal $-CO_2H$ Groups. Both the AFM and IRS data are fully consistent with a ≤50% MHA adlayer. First, the AFM images (Figure 8d) show a clear presence of island structures. Second, the IR spectrum (Figure 11, spectrum F) exhibits features very different from those of the bare MHA SAM (A) which can be interpreted in terms of relatively loosely packed adlayer chains with enhanced terminal group interactions.

In particular, the high-frequency region of the MHA|MHA bilayer (F) exhibits strong O−H stretching vibrations, seen as the broad 2500−3300 and 2500−2700 cm^{-1} features,[28] while the C═O stretching mode, a ∼1741 and 1719 cm^{-1} doublet for the MHA SAM (A), exhibits nearly a singlet shape dominated by the H-bonding $\nu_{C=O(H)}$ mode at ∼1719 cm^{-1} (F). A low adlayer density, even if distributed as small islands, would allow a high degree of conformational flexibility of the $-(CH_2)_{15}CO_2H$ moieties, thus enabling the carboxylic acid groups to gain the energetics of increased intermolecular H-bonding and thereby create a more hydrophilic surface for H_2O adsorption. In addition, an analysis of the C−H mode behavior, made by examining difference spectra of the final MHA|MHA bilayer and the starting MHA SAM (difference spectra not shown), shows the appearance of d^+ and d^- components at 2855 and 2923 cm^{-1}, significantly

(59) With deposition times above 2 h, the presence of free thiol at 164 eV can sometimes be seen in the sulfur XPS spectra, an indication of significant amounts of physisorbed hexadecanethiol on the surface.

(60) We also note that with longer solution deposition times (up to 24 h) impurity signatures increasingly begin to appear in the IR spectra which can be associated with adsorption and trapping of organic materials such as solvent and ambient contaminants.

(61) The size estimates are made with ChemBats3D Ultra software. The distances from the sulfur atom to the farthest hydrogen are used for comparison. For hexadecanethiol the distance from S to H_{33} is 21.3 Å; for 16-mercaptohexadecanoic acid it is 22.3 Å.

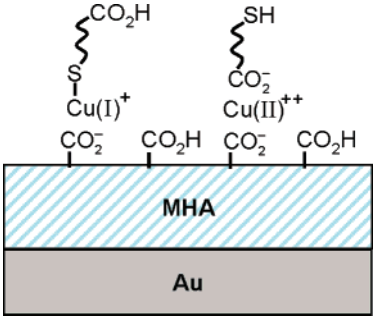

Figure 12. Schematic showing two possible attachment arrangements for an MHA bilayer on Au. The alkyl chains are shown schematically with no implications of a specific orientation or extent of conformational ordering.

shifted from the positions of 2852 and 2919 cm^{-1} in the pure MHA SAM and thus indicative of a highly conformationally disordered component. Since the MHA underlayer exhibits the same extent of conformational ordering (Figure 3) in the MHA SAM and MHA|MH bilayer, the disordering in the MHA|MHA bilayer is assigned to the MHA adlayer. We conclude that the significantly higher extent of disordering of the MHA adlayer compared to an MH adlayer (see section 3.1.4) is driven by the propensity of the MHA adlayer terminal $-CO_2H$ groups to form H-bonding networks. This is further facilitated by the relatively low coverage of the adlayer (~50%), which allows significant disorder of the chains as needed to provide maximum H-bonding.

3.2.1.2. Copper Coordination in MHA Adlayers: −SH vs $-CO_2H$ Attachment. In the case of the MH adlayer only S−Cu attachment is possible. For $-CO_2H$-terminated thiols, however, inverted attachment via $-CO_2H$ ligation with chemisorbed Cu^{2+} ions is also possible, as depicted in Figure 12.

While a previous report based on XPS results suggests that such inverted attachment does not occur,[8,9] we, however, find evidence to the contrary, as seen by comparing the IR spectra of the carboxylate and the carboxylic acid regions for the first three steps of growth for both the MH and the MHA adlayers (Figure 13).

Note that in the MH adlayer case (Figure 13, spectrum C) the original $\nu_{(CO_2^-)}$ features (~1440 and 1600 cm^{-1}) are gone while in the MHA adlayer case (Figure 13, spectrum F) these features remain to some extent,[62] an indication that while the intensity of both the $\nu_{s(CO_2^-)}$ and $\nu_{a(CO_2^-)}$ peaks decreases in the MHA adlayer, the area ratio changes dramatically, particularly as compared to the case of initial addition of Cu^{2+} to the MHA SAM (Figure 13, spectrum B). Under our IR reflection conditions with a surface selection orientation rule,[27] this change in relative intensity is likely caused by a change in the orientation of the $-CO_2^-$ oscillators. Upon coordination of an adjacent pair of $-CO_2H$ terminal groups in the SAM surface plane with a Cu^{2+} ion, the resulting $-CO_2^-$ orientations are expected to be roughly midway between having the O−C−O bisector angle normal to the surface and having the O−O axis normal to the surface, as depicted schematically in Figure 14a. This type of structure allows both $\nu_{s(CO_2^-)}$ and $\nu_{a(CO_2^-)}$ modes to be IR active since both have transition dipole moment (TDM) components perpendicular to the surface (refer to TDM directions in Figure 14c).

On the other hand, if MHA adlayer $-CO_2H$ groups were to coordinate with the preformed Cu^{2+} surface layer, one would expect the resultant $-CO_2^-$ moieties to tend toward alignment of their C_{2v} axes perpendicular to the surface (Figure 14b), thus

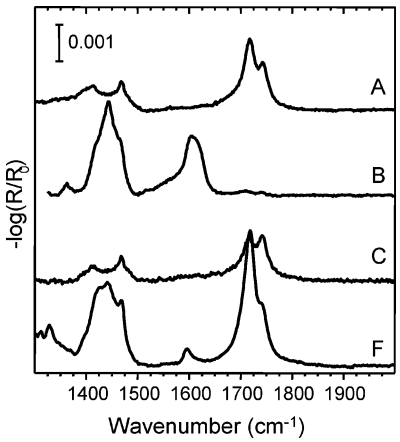

Figure 13. Infrared spectra for the first three steps of film stack growth. The spectra are labeled according to the sample resulting from a given step in Table 1. (A) Spectrum of the MHA monolayer showing the carboxylic acid stretching mode features. (B) Spectrum of the Cu^{2+}-coordinated MHA SAM (MHA−Cu) showing complete disappearance of the carboxylic acid features and appearance of carboxylate features. (C) Spectrum of the MHA|MH bilayer, formed by addition of an MH adlayer to the MHA−Cu surface. Note the complete loss of both carboxylate stretching modes and appearance of the carboxylic acid features. (F) Spectrum of the MHA|MHA bilayer formed by addition of MHA to the MHA−Cu surface. Note the presence of both carboxylate and carboxylic acid features.

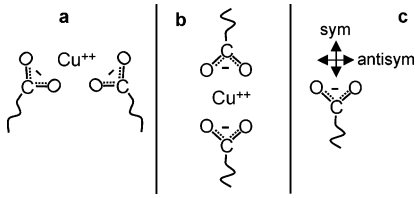

Figure 14. (a) Schematic of the general orientation of the copper carboxylate complex formed on the surface after the initial addition of Cu^{2+} ions to an α,ω-mercaptoalkanoic acid SAM. The SAM surface is implied to run parallel to the line connecting the carboxylate groups. (b) Schematic of the linear structure of a copper carboxylate complex which typically results when one or both carboxylate species are unconstrained geometrically. (c) Directions of the transition dipole moments for the symmetric and antisymmetric vibrations of a carboxylate ion with C_{2v} symmetry. The alkyl chains are shown schematically and not meant to imply any specific degree of conformational ordering or segment orientation.

allowing only the $\nu_{s(CO_2^-)}$ mode to be observed. The observed spectrum (Figure 13, spectrum F) shows a strong $\nu_{s(CO_2^-)}$ feature (~1440 cm^{-1}) and a weak $\nu_{a(CO_2^-)}$ feature (~1600 cm^{-1}), consistent with a generally perpendicular orientation of the C_{2v} axis but with a slight tilt.[63] The presence of these peaks supports the conclusion that a significant fraction of the adlayer molecules are attached via the $-CO_2^-$ moiety at the MHA|MHA interface.

The XPS results corroborate this conclusion. The Cu $2p_{3/2}$ spectrum (Figure 15, spectrum F) for an MHA|MHA bilayer (30 min of MHA solution immersion) shows that significant amounts of Cu(II) are present, in contrast to the case of MH layer formation (Figure 7, spectrum C) where all the Cu(II) was reduced to Cu(I).

This result is attributed to formation of $Cu^{2+}(CO_2^-)$ ionic complexes with the adlayer MHA molecules. Even if thermochemically unfavorable compared to reduction by −SH, rapid initial ionic complexation of MHA molecules would be expected to impede subsequent reduction reactions.

(62) It is possible that some of the adlayer did not react with the copper, thus forming an incomplete adlayer; however, longer deposition times did not reduce these peaks significantly.

(63) Without knowing the surface density of these adsorbates and the problems with the overlapping CH wagging modes, it is difficult to determine an accurate orientation.

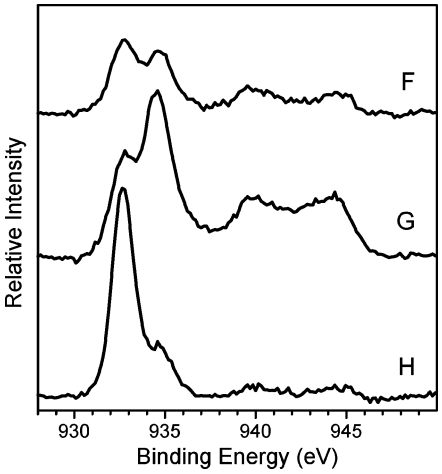

Figure 15. XPS Cu $2p_{3/2}$ region spectrum for the F−H stages of growth for a trilayer film.

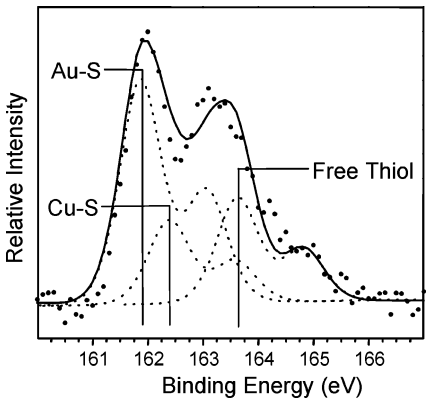

Figure 16. XPS S 2p region spectrum of an MHA|MHA bilayer sample. The experimental spectrum (heavy dots), three-component curve fits (light dots), and total fit envelope (solid line) are shown.

Further evidence of the mixed chemistry at the MHA|MHA interface is suggested by the S 2p XPS spectrum (Figure 16) of the bilayer sample where Au−S, Cu−S, and free −SH (at 161.9, 162.4, and 163.5−164 eV, respectively) features can be identified.

Due to the proximity of the binding energies of the three species, it is difficult to determine an accurate estimation of the proportion of each component, but an approximate fit of the components is shown in Figure 16. Importantly, the observation that no significant change is observed in either the IR or XP spectra for solution deposition times beyond ∼2 h indicates a stable state (kinetically or thermochemically) of a mixed attachment interface.

3.2.2. Cu^{+2} Ions Will Add to a Major Fraction of the Uncoordinated CO_2H Groups of an MHA|MHA bilayer (B → F). Samples of preformed MHA|MHA bilayers were immersed in 5 mM $Cu(ClO_4)_2$/ethanol solution for varying times from 5 to 180 s. Data are given for 30 s unless otherwise specified.

The Cu $2p_{3/2}$ XPS spectrum clearly shows the appearance of a Cu(II) signal. In comparison with the corresponding experiment with the MHA|MH bilayer, the MHA|MHA Cu(II) bilayer signal is significantly larger (see Figures 15, spectrum G, and 17, spectrum F). The IR spectrum (Figure 11, spectrum G) shows a distinct loss of the −O−H stretching mode features (2500−3300 and 2500−2700 cm^{-1}). The $\nu_{C=O(H)}$ and $\nu_{C=O}$ features (1718 and 1741 cm^{-1}) are greatly reduced in intensity, while the $\nu_{s(CO_2^-)}$ and $\nu_{a(CO_2^-)}$ mode intensities (1440 and 1600 cm^{-1}) increase. The $-CO_2H$ peaks, however, never completely disappear, even with extended Cu^{2+} solution deposition times, an indication that

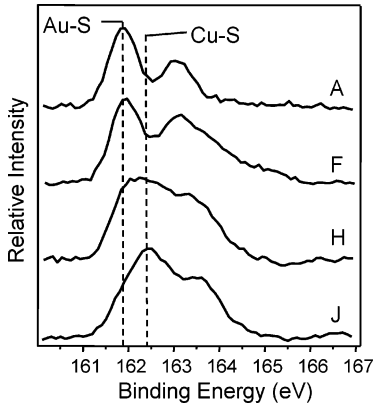

Figure 17. XPS S 2p spectra for steps A, F, H, and J of growth for a trilayer film. The dashed lines mark the peak positions of the Au−S and Cu−S species.

a fraction of the $-CO_2H$ groups, presumably those in the interior MHA|MHA interface, are difficult to access by the Cu^{2+} ions. As with the case of the MHA|MH bilayer, the second addition of copper causes a decrease in the adlayer coverage, as shown by intensity losses of d^+ and d^- and C 1s features in the IR and XP spectra, respectively.[64]

3.2.3. Formation of an MH Capping Layer on an MHA|MHA−Cu Bilayer (G → H) Involves Loss of Some Middle Layer MHA Molecules and an Incomplete Capping Layer Coverage. The MHA|MHA−Cu samples were placed in ∼5 mM MH or DMH (deuterated MH) solutions in ethanol for varying times from 10 min to 24 h. The results are given for 2 h unless otherwise stated.

Relative to the starting MHA|MHA−Cu bilayer, the XPS Cu $2p_{3/2}$ region shows a Cu(II) decrease (shoulder at 934.5 eV) and a Cu(I) increase (compare spectra G and H in Figure 15).[65] Comparison of the S 2p XPS core level spectra of the starting MHA SAM and the MHA|MHA bilayer (Figure 17, spectra A and F) with that of the corresponding MHA|MHA|MH capped trilayer (Figure 17, spectrum H) shows a significant increase in the Cu−S component (162.4 eV) relative to the Au−S component (161.9 eV) upon formation of the trilayer. In general, these data are consistent with a thiol reduction of Cu(II) to Cu(I) and protonation of $-CO_2^-$ to $-CO_2H$ (eq 2). The thiol−Cu(II) redox reaction is confirmed by the return of the IR $\nu_{C=O(H)}$ and $\nu_{C=O}$ features (∼1717 and 1742 cm^{-1}, Figure 11, spectrum H) after the MH adlayer forms. The reduction in the broad O−H stretching mode peaks (∼2800−3400 cm^{-1}) indicates a change in the mix of $-CO_2H$ and $-CO_2^-$ groups at the MHA|MHA interface.

The final SWE total thickness of the MHA|MHA|MH trilayer is 48 ± 2 Å (see Table 3), significantly lower than the ∼60 Å value estimated on the basis of an ideal, densely packed C16 chain trilayer.[8,9] The diminished thickness implies a relatively low coverage of the third layer. This can be understood by immersion of the MHA|MHA bilayer in DMH solution to see how the deuterated molecules are incorporated. Comparison of the C−D stretching mode features in spectra G and H in Figure

(64) It is unclear whether the free thiols on the inverted MHA molecules react with the copper and allow for the formation of an additional adlayer at that site. Previous work on dithiol multilayers suggests that such a site would be active for adlayer formation.[10] Our experimental methods do not allow any definitive conclusion regarding further addition, but if it did occur, as expected, it would contribute to "roughening" of the multilayer structure by formation of islands of chains at the terminal layer of the multilayer stack with deterioration of the "molecular ruler" characteristics.

(65) We were unable to determine the amount of Cu(II) and S in the MHA|MHA|MH film relative to the MHA|MHA bilayer due to the complexity of the trilayer structure in terms of modeling the attenuation of the photoelectron fluxes. Also, X-ray beam induced Cu(II) autoreduction made the Cu analysis somewhat problematic.

11 shows incorporation of DMH molecules. A C−H intensity decrease, however, also indicates some MHA molecule loss, presumably due to exchange with DMH molecules, thus placing some fraction of the DMH molecules in the middle layer of the MHA|MHA|DMH structure and yielding a mixed $-CO_2H/-CH_3$ surface with a reduced number of attachment sites for the capping adlayer. At best, according to the redox attachment reaction in eq 2, the capping layer would have ∼50% coverage (based on the foundation SAM); any MH → MHA displacement would further reduce this value.

3.2.4. Densification of the Incomplete MHA|MHA|MH Trilayer by Readdition of Cu^{2+} and MH Molecules (H → J). By repeating the Cu^{2+} and MH addition steps a denser multilayered structure can be formed in the same manner as previously with the MHA|MH bilayer structure (section 3.1.5). Immersion of the initially formed MHA|MHA|MH trilayer in Cu^{2+} solution leads to a loss in the intensity of both the C−D and C−H stretches in the IR spectra (data not shown), consistent with a loss of material in both the second and third adlayers. Reimmersion in MH solution gives a final SWE thickness of 56 ± 2 Å, 8 Å thicker than the initially formed trilayer (compare spectra H and J in Table 3) and an indication of ∼15−20% densification of the stack.[66] In general, further densification is possible but after several immersions tends to reach a limiting value near ∼25−30%.

3.3. General Observations on the Effects of Odd−Even α,ω-Mercaptoalkanoic Acid Chain Length Variations. A series of similar bi- and trilayer formation experiments were performed using the odd chain MPA molecule. Since the details are quite similar, they are not presented, but in general, the MPA-based stacks showed larger variations in the reproducibility of the data than for the even MHA molecule stacks, particularly when longer solution times were used. For example, the total thicknesses of multilayers ranged by ±5 Å instead of ±2 Å. The basic issue appears to be that the odd MPA CO_2H chain surface leads to a CO_2H orientation that allows typical impurities (e.g., fatty acids) to adsorb more easily than for the even MHA chain. This behavior tends to produce lower packing densities in the adlayer growths than for the even MHA SAM. It may be that rigorous preparation conditions could avoid this, but even extra care did not prevent the problem in our hands.

4. Conclusions and Perspective

The main conclusion from our study is that a growth mechanism for Cu^{2+}−mercaptoalkanoic acid multilayer films is operating that is different from that previously proposed[8,9] with important implications for making accurate predictions of the multilayer film thicknesses, critical to molecular ruler applications. In addition, a method is demonstrated that aids in densification of incomplete coverage structures, thus allowing more accurate and reproducible control of the final film structures, particularly thicknesses and density fluctuations.

The main features of the film growth can be summarized as follows. For reference, the first several steps are depicted schematically in Figure 18.

The first step, Cu^{2+} ion addition to a foundation SAM prepared from α,ω-mercaptoalkanoic acid self-assembly on Au, proceeds quantitatively to form a surface layer of composition $(-CO_2^-)_2$-Cu^{2+}. Immersion of this surface in a capping layer of mercaptoalkane induces a redox reaction to form an overlayer of [RS−Cu^+](−CO_2^-), where R is the overlayer alkyl moiety. The 1:1

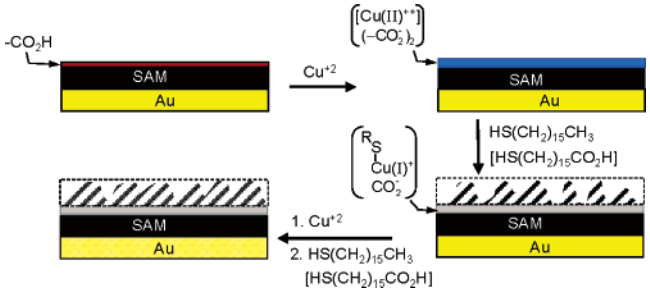

Figure 18. Schematic illustration of the initial steps in forming a Cu-ligated α,ω-mercaptoalkanoic acid multilayer stack with major features of the structures as characterized in our experiments.

R:Cu stoichiometry results in a ∼50% coverage of the overlayer relative to the foundation SAM coverage. AFM and IRS results show that this coverage is distributed as discrete islands with the R chains exhibiting substantial conformational order, thus implying aggregation of chains, perhaps in "tuftlike" structures. When the mercaptoalkanoic acid is used to form the second layer, a similar Cu(II) → Cu(I) redox reaction occurs with the adlayer thiols but with additional complications from a small fraction of adlayer molecules inverting to bind their $-CO_2H$ group to the surface Cu^{2+} ions via formation of an ionic $(RCO_2^-)_2Cu^{2+}$ complex. While the incomplete adlayer coverage can be increased by continued cycles of Cu^{2+} complexation of available $-CO_2H$ groups followed by RSH chemisorption, the coverage does not reach 1:1 with the foundation SAM coverage, and our AFM topography images indicate significant island formation. Further, continued immersion cycles tend to progressively disrupt the films past the first few cycles. As additional layers are added to the multilayer stacks, the integrity of the interlayer binding becomes increasingly disrupted with mixtures of [RS−Cu^+](−CO_2^-) binding and the inverted molecule $(RCO_2^-)_2Cu^{2+}$ binding. It can be expected that the islanded topography that initiates in the first steps to the bilayer formation will continue to propagate during growth to produce a final topographically rough surface with a total stack thickness significantly below the theoretical value defined by integral multiples of the molecular thicknesses based on their values for pure SAMs.

Finally, a comparison of odd and even chain length α,ω-mercaptopentadecanoic and α,ω-mercaptohexadecanoic acid molecules in multilayer structures shows the same chemical reactions and similar resultant structural formation. However, the odd chains were found to be significantly more prone to contamination and did not generally build multilayer structures as reproducibly as the even chains, though with care in surface cleaning and contamination control the results could be somewhat improved.

Overall, our results suggest that in molecular ruler lithography applications significant care must be taken in the design of target structures with expected thicknesses and line edge roughnesses based on predicted characteristics of Cu-ligated mercaptoalkanoic acid stacks. Since the Cu binding chemistry with attendant adlayer coverage issues is inherent in these films, the use of other interfacial attachment chemistry or the use of highly controlled polymer brush structures could offer alternative ways to make more accurate spacer films, and work is under way in our laboratories toward this end.

Acknowledgment. We acknowledge funding from the NSF-funded Pennsylvania State University Center for Nanoscale Science (MRSEC Grant DMR-0080019).

LA0621719

(66) Unfortunately, with the densified trilayer sample point the overlayer thickness becomes too large to allow useful interpretations of the XPS Au−S S 2p core level spectra. This can be seen in Figure 17, spectrum J, where the Cu−S species dominate with only a shoulder of the Au−S observable.